

**TEMPERATURE CLIMATOLOGY OF THE MIDDLE  
ATMOSPHERE FROM LONG-TERM LIDAR MEASUREMENTS  
AT MID- AND LOW-LATITUDES.**

Thierry Leblanc <sup>1</sup>, I. Stuart McDermid <sup>1</sup>, Philippe Keckhut <sup>2</sup>, Alain Hauchecorne <sup>2</sup>,

Ciao Y. She <sup>3</sup> and David A. Krueger <sup>3</sup>.

<sup>1</sup> Jet Propulsion Laboratory  
California Institute of Technology  
Table Mountain Facility  
Wrightwood, CA 92397

<sup>2</sup> Service d'Aéronomie du CNRS  
Verrières-le-Buisson  
91371 Paris, France

<sup>3</sup> Department of Physics  
Colorado State University  
Fort Collins, CO 80523

Submitted to the Journal of Geophysical Research-Atmospheres, November 1997

## Abstract

Long term measurements from several lidar instruments (Rayleigh and sodium) located at 44.0°N, 40.6°N, 34.4°N, and 19.5°N have been used to develop a new climatology of the middle atmosphere temperature. For each instrument, the measurements on every individual day of the year over the entire long-term record were averaged to build a composite year of temperature profiles. These profiles were then interpolated to provide temperature values at 1 km altitude intervals so that the climatology comprises daily temperature values at integer altitudes between 15 and 110 km, depending on the instrument. The climatologies for each lidar were then compared to the CIRA-86 model and to each other. Large differences between the lidar temperatures and the CIRA-86 temperatures are identified and explained. When compared to all instruments, CIRA-86 seems systematically much too cold between 90 and 95 km, by 20 K or more, and possibly 6-8 K too warm around 80 km, making its use as a reference atmosphere model questionable at these altitudes. The annual and semi-annual components of the seasonal variability and the 2- to 33-day period variability were investigated. An annual cycle with 6-7 K amplitude in the upper stratosphere, increasing to 15-20 K at 80 km, is observed at mid-latitudes. This cycle is in phase with the solar flux in the stratosphere and in opposite phase in the mesosphere with a very cold summer mesopause at 85 km, in good agreement with previous climatologies. At lower latitudes, a semiannual oscillation (SAO) propagates downward from 85 to 30 km and is characterized by a stronger first cycle than the second (4 K and 2 K amplitude respectively). The 2- to 33-day variability at mid-latitudes shows a maximum during winter around 40 km and in the mesosphere. The first peak is associated with planetary wave activity and stratospheric warmings, and the second to the occurrence of mesospheric temperature inversions. Finally, sudden seasonal transitions, highly consistent between all instruments, have been observed. In particular, in the early winter mid-latitudes a two-step warming of the winter mesosphere between 65 and 85 km as well as a cooling of the lower mesosphere appear to be real climatological events rather than some short-term geophysical or instrumental random variability.

## 1. Introduction

The temperature structure of the middle atmosphere has been studied for several decades. The first investigations used rocketsondes and falling spheres to measure temperature profiles up to 60–90 km but with relatively poor accuracy due to uncertain radiative and aerodynamic heating corrections [Schmidlin, 1981]. *Elterman [1951]* had the idea to measure the atmospheric density using Rayleigh backscattering. The first experimental [Kent and Wright, 1970] and systematic [Hauchecorne and Chanin, 1980] temperature profiles derived from Rayleigh lidar measurements of the relative density of the middle atmosphere provided improved vertical resolution and accuracy. Unfortunately, most of the ground-based methods cited above made measurements above lands located in the northern mid-latitudes. The crucial need for a better horizontal coverage, especially for low-latitudes, ocean areas, and the southern hemisphere, led to the development of satellite measurements. The Pressure Modulated Radiometer (PMR) [Curtis et al., 1974] in the seventies, together with the Limb Infrared Mesospheric Sounder (LIMS) [Gille et al., 1984], the Stratospheric And Mesospheric Sounder (SAMS) [Rodgers et al., 1984], the Stratospheric Sounding Units (SSU) [Miller et al., 1980], and the Solar Mesosphere Explorer [Clancy and Rusch, 1989] in the eighties, progressively obtained global coverage of the middle atmospheric temperature profiles. However, the vertical resolution of the satellite measurements remained poor compared to most of the ground-based instruments. More recently the Upper Atmosphere Research Satellite (UARS), launched in September 1991 and especially dedicated to the study of the middle atmosphere, carried four instruments to measure stratospheric and lower mesospheric temperatures: the Microwave Limb Sounder (MLS) [Fishbein et al., 1996], the Cryogenic Limb Array Etalon Spectrometer (CLAES) [Gille et al., 1996], the Halogen Occultation Experiment (HALOE) [Russell et al., 1996], and the Improved Stratospheric And Mesospheric Sounder (I SAMS) [Taylor et al., 1996]. Some of these instruments are still operating to this date, providing one of the most extensive satellite data sets ever obtained, but still with a poor vertical resolution characteristic of the passive remote sensing methods used

Currently, lidar measurements provide the best vertical resolution and accuracy for middle atmosphere temperature studies (stratosphere and mesosphere, -15 to -100 km). Also, they can provide long-term data series relatively absent of instrumental drift and an integration of the measurements over several hours removes most of the gravity wave-like short scale disturbances. Lidar is thus one of the most suitable instrument for studying variations of the middle atmosphere temperature on various time scales [Derr and Little, 1970]. This paper will describe a seasonal climatology of the middle atmosphere temperature derived from lidar measurements obtained at several mid- and low-latitude locations. Results from the following lidars, which have all obtained a long- or at least mid-term measurements record, were used in this study: the two Rayleigh lidars of the Service d'Aéronomie du CNRS, France, located at the Observatoire de Haute Provence (OHP, 44.0°N) and at the Centre d'Essais des Landes (CEL, 44.0°N), the two Rayleigh lidars of the NASA-Jet Propulsion Laboratory, USA, located at Table Mountain, California (TMF, 34.4°N) and at Mauna Loa, Hawaii (MLO, 19.5°N), and the Colorado State University, USA, sodium lidar located at Fort Collins, Colorado (CSU, 40.5°N). The overall data set extends from 1978 to 1997 with different periods of measurements depending on the instrument. Three of the instruments are located at primary or complementary stations (OHP, TMF, MLO) within the Network for Detection of Stratospheric Change (NDSC). The NDSC network will soon include seven different latitude ranges, providing an extensive latitudinal coverage of

ground based measurements. After a short technical description of the instruments, data sets, and data processing, several aspects of the **temperature** climatology obtained by **lidar** in the middle at **mosphere** arc presented.. These include the **climatological temperature** average through the year; the differences compared to the **CIRA-86 climatological** model, a comparison **between** the **lidar** instruments, annual and semi-annual components of the climatology, and 2-to 33-day period variability.

## 2. Brief description of the **Rayleigh** and **sodium lidar** principles.

**Rayleigh** and **Raman** scattering: Laser radiation emitted at wavelength  $\lambda$  and transmitted into the atmosphere is **backscattered** by the molecules in the atmosphere and collected by a telescope at the same or a different wavelength. When the Mic scattering duc to the aerosols particles is negligible compared to the molecular scattering (i.e. above 30 km) the number of photons **received** from a scattering layer  $\delta z$ , at a mean altitude  $z$ , is proportional to the number of photons emitted in the laser pulse and to the number of air **molecules** (or air density). For **Rayleigh** scattering the emitted and received wavelengths arc **the** same. Assuming that the only non-negligible absorption in the atmosphere is duc to ozone, the atmospheric density can be derived from **the Rayleigh lidar** equation and written:

$$p(z) = N(z) K \frac{(z - z_0)^2}{\delta z} \exp(2\tau_{Ray}(\lambda, z) + 2\tau_{O_3}(z, z_0)) - n(z) \quad (1)$$

where  $N(z)$  is the number of photons **received**, per laser pulse, from altitude  $z$  by a **telescope** at altitude  $z_0$ .  $\tau_{Ray}$  and  $\tau_{O_3}$  are **the** optical thickness integrals for the **Rayleigh** extinction and the ozone absorption **between** the altitudes  $z_0$  and  $z$ .  $K$  is an undetermined proportionality constant **dependent** on instrumental parameters,  $n(z)$ , is the number of photons coming from **the** natural sky background light added **to** the photon and electronic noise from **the** counting system. For vibrational **Raman** scattering the scattering process, the cross sections, and **the received** wavelength (**backscattered** by the nitrogen molecules) arc different [e.g. *Keckhut et al.*, 1990]. Consequently, the transmission terms  $\tau_{Ray}$  and  $\tau_{O_3}$ , and the constant  $K$  in equation (1) have different values. The vibrational **Raman** scattering is roughly 1000 times weaker than the Rayleigh scattering but is relatively insensitive to aerosols making it useful to obtain temperatures at lower altitudes (typically between 15 and 35 km). After subtracting the noise from the **Rayleigh** or **Raman** signal, the temperature is **deduced** from the relative density (i.e., the unknown constant  $K$  is not required) using **the** hydrostatic equilibrium and **ideal** gas law assumptions [*Hauchecorne and Chanin*, 1980]. A priori temperature information is needed at **the** top of the profile and is usually taken from **climatological** models like **CIRA-86**. The total error in the temperature at the top due to this a priori initialization can be larger than 20 K but rapidly **decreases** as the **temperature profile** is integrated downward (typically divided by a factor of 3 every 10 km). Detailed reviews of the different sources of temperature uncertainty arc given for example in [*Donovan et al.*, 1993, *Keckhut et al.*, 1990, and *Leblanc et al.*, 1997].

**Sodium layer laser-induced-fluorescence**: The two-frequency, narrowband Na temperature **lidar** system relies on laser-induced-resonance-fluorescence from naturally occurring sodium atoms in the **mesopause** region. Since the sodium resonance-fluorescence is -14 orders of magnitude stronger than the **Rayleigh** scattering, even a **lidar** with a modest power-aperture product is capable of obtaining profiles with good signal-to-noise. The operating principle of

this lidar has been described in detail for example by [She *et al.*, 1992]. Briefly, laser-induced-fluorescence intensity profiles are measured at excitation frequencies that are sensitive to temperature changes; the  $D_{2a}$  peak and cross-over Doppler-free resonances, respectively, at  $\nu_a = -651.4$  MHz and  $\nu_c = 187.8$  MHz measured relative to the Na  $D_2$  transition at 589.158 nm. The return profiles for a predetermined time interval are measured alternately at the two excitation frequencies  $\nu_a$  and  $\nu_c$ . The measured profiles are first background corrected and then normalized to Rayleigh scattering at 30 km. For this climatological study, the normalized and background-subtracted photocount profiles,  $I_c$  and  $I_a$ , integrated throughout the night are averaged separately for each frequency. After the nightly mean signal profiles have been vertically smoothed (typically few kilometers) a ratio profile,  $RT(z) = I_c / I_a$ , is calculated. Nightly mean temperature profiles are then deduced from the ratio profile  $RT(z)$ .

### 3. The instruments, database and data processing:

At mid-latitudes, the CNRS-SA Rayleigh lidar at OHP (44.0°N, 6.0°E) has obtained measurements between 30 and 95 km from 1978 to the present with 75 to 300 m vertical resolution, and that at CEL (44.0°N, 1.0°W) from 1986 to 1994 with 300 m vertical resolution. Profiles are obtained during the entire night if the weather conditions are good (no cloud, and weak wind). This gives an average of 5-6 hours integration of nighttime measurements, about 4-5 days a week (150-200 profiles per year). The total estimated temperature error at the top of each profile is about 20-25 K, including a priori initialization and statistical noise. This error drops to less than 1 K at mid-range (typically 55 km) and below. The CSU(40.6°N, 105.1°W) Na lidar has obtained mesospheric temperature measurements in the Na layer between 80 and 110 km since 1993 with an initial 75 m vertical resolution smoothed over 3 km. Quality, regular nighttime temperature measurements, i.e., on average four to five nights a month with 4 hours or more observations each night, were started in May 1993. Observations on nights with good winter weather conditions occasionally lasted longer than 11 hr and statistically observations were evenly distributed throughout the night. The total estimated temperature error is less than 5 K and 9 K at the top and bottom of the profiles respectively, dropping to 0.6 K at mid-range (typically 90 km).

At lower latitudes, the NASA-JPL Rayleigh lidars [McDermid *et al.*, 1995] located at TMF (34.4°N, 117.7°W) and MLO (44.0°N, 155.6°W) have obtained temperature measurements between 30 and 80 km since 1988, and between 15 and 90 km since 1993 respectively. Most of the “routine measurements” comprise a 1.5-2.0 hour integration experiment, usually at the beginning of the night 4-5 nights a week, insuring a good survey of stratospheric ozone and temperature as required by the NDSC program. The associated temperature errors are similar to that of the French Rayleigh lidars, but the top of the profiles are slightly lowered. To avoid any confusion of definitions, MLO will be considered hereinafter as a “tropical” latitude site and TMF as a “sub-tropical” latitude site in contrast with the other sites located at “mid-latitude”.

For all instruments, each individual temperature profile was interpolated to obtain data points every one kilometer thus making the data analysis and the comparisons between instruments easier. Table 1 illustrates some basic characteristics of each instrument together with the corresponding data sets used in this study (individual profiles). The most complete database was obtained at OHP, then TMF and CEL, then MLO and CSU. For some instruments with a long period of measurements the oldest years were not used as noted in table 1. This applies to OHP (starting

measurements in 1978 but using 1984 as the **first** year) and **TMF** (starting in 1988 but using 1990 as the first year). There are **two** main reasons for not using the entire database. 1) For **OHP**, there **were** only a limited number of measurements during the years 1978-1983 so that omitting these years does **not** lose much information. Also, it is interesting to compare the current climatology (1984 - 1995) with that previously obtained for the period 1978-1989 by *Hauchecorne et al.* [1991]. 2) For both **OHP** and **TMF**, the results obtained during the first months or years of measurements and certainly before processing to an “operational routine mode” were considered experimental or preliminary and may have been affected by instrumental changes, and/or by some noisy profiles. This is not the case for **MLO** since the **lidar** group in charge with this instrument is the same as for the **TMF** instrument (**NASA-JPL**). As shown in **Table 1**, the top of the profiles was truncated about 10 km lower than the initial cut-off altitudes cited above. This way, the results containing a non negligible part of “a priori” information and/or noise will not be shown and the resulting statistical error drops by at least a **factor 3**. For all instruments this error is still high (-5 K) but the long period and/or the large number of measurements for most of the instruments will reduce it to few **Kelvins** for the composite daily and monthly mean profiles. High confidence levels are expected up to 75 km altitude. Also, the bottom of the **TMF** profiles was truncated at 32 km instead of 30 to avoid any direct effect of volcanic aerosols, especially after the eruption of **Pinatubo** (eruption in June 1991, major effect in spring-summer 1992). For **CSU**, depending on photon noise, typical measurement accuracy for the nightly mean temperatures are -0.6 K near the peak (92 km) and -4 to 8 K at the edges (80 km and 108 km) of the Na layer. Thus, unlike **Rayleigh** and **Raman** scattering whose accuracy decreases as altitude increases, the sodium **lidar** measurement is most accurate near 92 km where the sodium density peaks. Although temperature measurements were typically made between 80 and 110 km at Fort Collins, Colorado, the hours of observation and altitude ranges covered are shorter in summer due respectively to shorter nights and lower Na densities compared to winter. **Therefore**, only **CSU** profiles **between** 84 and 105 km are used for this **climatological** study. At **OHP**, **CEL**, **TMF** and **MLO**, the **effect** of the **Pinatubo** eruption (June 1991) was observed in the **profiles** below -30 km, The **total** number of profiles obtained per month is highly variable, depending on the instrument.

#### 4. Data analysis and results

##### a. Climatological temperatures

For each instrument, all individual temperature profiles (from 249 to 1244 profiles depending on the instrument, see Table 1) were merged into a composite single year of data, A weighted running average with a triangular 33-day width filtering **scheme** was applied to each day of the composite year that a profile was available. The remaining days with no profile were filled with an interpolated profile obtained using a two-dimensional minimum **curvature** spline surface method. Although these interpolated profiles were plotted, they were not retained in the numerical database in order to avoid inaccuracies in the different analysis steps described in this section. No removal of tidal structures was performed. At mid-latitudes, the **semidiurnal** tide is expected to be **dominant**, with a few **Kelvins** amplitude at 80 km, For **OHP**, **CEL**, and **CSU**, most of the measurements were taken over the entire night, minimizing the **effect** of the 12-hour oscillation, At **TMF**, where measurements are performed during 2 hours in routine mode, the top of the profiles is lowered to 75 km, and the **semidiurnal** amplitude has decreased significantly. At

MLO, the role of the diurnal and semidiurnal tides may not be negligible above 80 km, as well as the diurnal component at CSU above 90 km. The effect of tides will be discussed each time it is considered necessary.

The mean annual temperature climatologies obtained for OHP, CEL, TMF, CSU, and MLO are presented in **Plates 1a to 1d**. For case of comparison the color scale and the altitude range ( $z_{top}-z_{bottom}$ ) in these plates, and also most other plates in this paper, are identical for all instruments. A distinctly defined temperature pattern is observed at all sites. **Plate 1d (MLO)** clearly exhibits a semiannual cycle at the stratopause (maximum of 266 K at 47 km) and an annual cycle in the lower stratosphere with a very cold minimum of 190 K at 17 km, identified as the tropical tropopause. As expected at these latitudes, the amplitude of the seasonal variations is weak, At the top (80-85 km), where the effect of the mesospheric tides is the largest, the measured cold temperatures are more representative of early night temperatures than nightly (or even a 24-hours) mean temperatures,

For OHP, CEL and TMF (**Plates 1a to 1c**), a familiar mid- and subtropical latitude warm summer and cool winter stratosphere is observed with a maximum of 272 K in May-June and a minimum of 255 K in early November at the stratopause altitude of 47 km. A characteristic warm winter/cold summer mesosphere is also observed with a maximum of 220 K in December and January, and a minimum of 195-200 K in May-June at 75 km. For OHP, temperatures lower than 175 K are observed at 85 km in June-July, in good agreement with previous climatologies [Hauchecorne *et al.*, 1991] and 2-5 K colder than the 175-180 K measured by the Na lidar at Fort Collins (**Plate 1c**). The weak negative vertical temperature gradient observed in winter at OHP, CEL and TMF is the consequence of the seasonal average of the so-called mesospheric temperature inversions occurring during the entire winter at OHP and CEL, and more specifically in February at TMF. A more detailed description of the temperature inversions is presented in [Leblanc and Hauchecorne, 1997a]. The temperature pattern above CSU is not very different from that described by Yu and She [1995] in their first climatology. The main difference is in spring and fall, where the so-called “double temperature minimum” is no longer a significant part of the climatology. Instead, a continuously cooling layer in spring and warming layer in fall can be observed between 85 and 95 km. As for the temperature inversions, this can be interpreted as the result of the seasonal average. The double minimum is now only observable in early April. The most significant feature observed in **Plate 1c** is the evidence of a 2-state mesopause, as already reported by Yu and She [1995]. The “winter state” is characterized by a temperature minimum located about 103 km, with 2 absolute minima (185-190 K) in spring and fall. The “summer state” is characterized by a temperature minimum at 85 km, with an extremely cold summer mesopause (< 180 K). The transition between the summer and winter mesopause is short, taking less than two months (April-May and August-September) as already reported by Senft *et al.* [1994]. Another remarkable similarity between OHP, CEL, CSU and previous observations at Urbana (40°N, 88°W) [Bills and Gardner, 1993] is the total temperature difference of 40 K between winter and summer in the 85-95 km range. Despite the high variability reported at these altitudes (Bills and Gardner reported a 115 K maximum amplitude at 90 km) the calculated climatological temperatures are 210 K, 215 K and 220 K, in winter, and 170 K, 175 K and 180 K, in summer, at Urbana, OHP, and CSU respectively.

## b. Inter-comparison between OHP, CEL, and CSU

The composite daily mean profiles were averaged to obtain the climatological monthly mean temperatures. As shown in **Plate 2a**, the difference between OHP and CEL does not exceed 6 K between 70 and 80 km. Below 70 km this difference never exceeds 4 K, with typical values between  $\pm 2$  K. The differences observed here are explained by 1) an interannual variability, since OHP and CEL periods do not match perfectly, 2) a residual atmospheric variability, since the measurements are not necessarily simultaneous, and 3) a residual instrumental noise at the top of the profiles. The maximum of 6 K above 80 km in January-February can be considered as the extreme error in determining the climatological temperatures for both instruments at that height. Below 60 km this error drops to under 2 K. Since the results obtained at OHP and CEL are almost identical, data from both sites will be computed and plotted together, as a single mid-latitudes site (44°N) hereinafter called "OHP+CEL". Results from OHP and CEL will be shown separately only if significant differences are observed, or if there is a need for an inter-comparison.

The difference between the OHP+CEL temperatures and the CSU temperatures are shown in **Plate 2b**. The overlapped altitudes are initially 80-90 km, but the significant results actually appear between 83 and 87 km. In fact, the lower part of the CSU profiles is systematically too warm below 82-83 km due to the decrease in Na concentration and a consequent increasing uncertainty and systematic error in the Na lidar analysis method. Above 85 km, the OHP+CEL temperature profiles contain a non-negligible part of CIRA climatology due to the a priori initialization at the top. A negative difference is observed at 85 km and above in **Plate 2b**. This difference will be explained below when comparing the observed climatology to the CIRA-86 climatology.

## c. Difference from CIRA-86

The monthly mean lidar temperatures were subtracted from the monthly mean CIRA-86 climatological temperatures. The first temperature climatology was obtained using the early radiance measurements (1975-78) of the Pressure Modulator Radiometer measurements (PMR) aboard Nimbus 6 [Curtis *et al.*, 1974; Labitzke and Barnett, 1981], and the Selective Chopper Radiometer (SCR) aboard Nimbus 3 (1973-74) [Ellis *et al.*, 1973]. The CIRA-86 temperatures [Fleming *et al.*, 1990] were then derived up to 86 km from the Middle Atmosphere Program (MAP) model on one hand [Barnett and Corney, 1985], and from an extrapolation of the Mass Spectrometer Incoherent Scatter (MSIS-83) thermospheric model between 120 and 86 km on the other hand [Hedin, 1983]. The temperature difference between the observed lidar climatology and the CIRA-86 climatology is plotted in **Plates 3a** (OHP+CEL and CSU), **3b** (TMF) and **3c** (MLO). For convenience, and since they have quasi-separated altitude ranges, OHP+CEL and CSU are presented on the same plot (**Plate 3a**) with a separating altitude of 85 km,

The observed departures from the model have typically 3 origins. The first one is the usually small magnitude of the CIRA temperature variability, compared to the observed temperatures. In our case, this applies at mid-latitudes in the stratosphere, and in the mesosphere above TMF. This is partly due to the poor vertical and horizontal resolutions acting as dramatic smoothing when computing the CIRA temperatures, and partly due to residual noise and/or

variability when computing the observed temperatures. The associated errors remain small, in the order of 1-2 K, and can not be easily identified.

The second source of departure is related to a systematic error in the CIRA temperatures, also due to its poor or irregular horizontal resolution and a poor vertical resolution, or due to drifting measurements. Once again, this error remains small in the middle atmosphere but is not negligible since it can affect an entire layer or season. For OHP and CEL (**Plate 3a**), the observed temperatures are systematically 2-4 K colder than the CIRA between 30 and 40 km, especially in summer, and 2-6 K colder between 70 and 80 km, while no systematic error is observed at stratopause altitudes. These results are similar to those obtained previously by [Chanin *et al.*, 1990] and [Hauchecorne *et al.*, 1991] over an earlier period. For TMF (**Plate 3b**), no significant departure of this type is observed. For MLO (**Plate 3c**), the entire region between 15 and 55 km is colder than the CIRA (up to 4 K in the upper stratosphere), which is in good agreement with the previous SME-CIRA-86 comparisons at similar latitudes [Clancy *et al.*, 1994]. At mesopause altitudes this error is dramatically large at mid-latitudes, as illustrated by the difference CSU-CIRA (top of **Plate 3a**), where very large positive departure (more than 16 K) is observed in the entire mesopause region (90-95 km). Once again, Clancy *et al.*, [1994] reported similar SME/CIRA-86 departures, suggesting that the CIRA is definitely too cold at these heights and latitudes. Consequently, the temperature initialization using CIRA might lead to too cold temperatures at the top of the OHP and CEL profiles, providing an explanation of the negative difference observed between CSU and OHP+CEL at 85 km and above (**see Plate 2b**). This is confirmed when comparing the seasonal variation of the magnitude of the difference CSU - CIRA and that of the difference OHP+CEL - CSU: The maximum (+25 K) deviation between CSU and CIRA at 90-95 km is observed in April-May (**Plate 3a**), just when the (-9 K) maximum OHP+CEL - CSU departure occurs (**Plate 2b**). In the other hand, the minimum deviation CSU - CIRA occurs in February, just at the same time as the minimum departure between OHP+CEL and CSU (-2 K). Due to this "polluting" effect of an a priori information, the use of Na lidar or satellite (SME, UARS) climatological data is currently under investigation by the CNRS/SA and JPL lidar groups, for initializing the top of their Rayleigh temperature profiles.

The third source of error is related to transient processes, such as sudden seasonal transitions from summer to winter or stratospheric warmings. The CIRA temperatures have a 1-month time resolution and can not accurately take into account such processes with time scales shorter than 2-3 months. The associated errors are generally large. For OHP+CEL observed temperatures are up to 10 K colder than CIRA in December and January below 40 km. This can be explained by the out-of-phase occurrence, between late January and February, of stratospheric warmings at OHP and CEL, and its equivalent occurring earlier in the CIRA model (December-January). Consequently, the CIRA is too warm in December and January. In the lower mesosphere, OHP+CEL and TMF temperatures are warmer than the CIRA. A maximum departure of 10 K around 70 km is observed in February at TMF, 4 K at 60 km in April-May for all mid-latitudes sites, and 4 K (respectively 8 K) at 60-70 km in November above OHP/CEL (respectively TMF). In the middle mesosphere, OHP/CEL temperatures are colder than CIRA, with a maximum departure of 10 K in November at 75-80 km.

For MLO (**Plate 3c**), the temperature departures are smaller than at mid- and subtropical latitudes. This is not surprising since the variability is itself smaller at low-latitudes. Consequently, the errors due to the annual and semi-annual amplitudes, and the errors due to the seasonal transitions are minimized. In the entire middle atmosphere, except at two times of the year between 60 and 70 km, the CIRA is warmer. In the stratosphere, the systematic departure is about 2 K. At 80 km a maximum of 10 K negative departure can be observed. Also, a very special pattern is observed at the beginning of the year: A negative departure is propagating downward from 80 km, associated with a positive departure around 65 km, and a negative departure again between 50 and 55 km. The similarity in the downward propagation for these three different layers suggests a possible outward sign of a wavelike structure. In fact, the associated vertical wavelength is close to that of the diurnal tide (28 km for the first mode), suggesting that the temperatures measured by lidar at MLO are representative of early night temperatures. If so, the downward propagation observed in **Plate 3c** might be a consequence of the seasonal variation of the tidal phase. A non-negligible role of the Semiannual Oscillation (SAO) may also account for such a structure as well. A longer database at MLO is anyway necessary to provide a more detailed explanation. Whatever is the source of departure between the lidar observations and the CIRA-86 model, it has to be noted that these departures are in very good qualitative agreement with those reported in [Clancy *et al.*, 1994] (see for instance their figures 6 and 7, and compare to our **Plates 3**). Quantitatively, some differences of few Kelvins remain, but this can easily be explained by the different vertical resolutions of the SME and lidar instruments, and by a non-negligible interannual variability.

#### d. Temperature deviations from the annual mean

The annual mean temperature profile was then subtracted from each available daily composite profile. Thus, the composite daily deviation from the annual mean was obtained. **Plates 4a to 4c** represent this deviation for OHP+CEL, CSU, TMF, and MLO. As expected for OHP+CEL, CSU, and TMF (**Plates 4a and 4b**), an annual cycle is clearly dominant in both the stratosphere and mesosphere. At 67-70 km, its phase compared with the solar flux is inverted leading to the classic warm summer stratosphere and cold summer mesosphere and vice-versa in winter. A second phase inversion is clearly observed at CSU (top of **Plate 4a**) around 95-100 km, marking the transition between the dynamically and chemically or radiatively driven upper mesosphere. These plates, in particular **Plate 4a**, also exhibit a warm late winter centered at 35-40 km. This is the signature of the stratospheric warmings occurring from January to March at mid- and high-latitudes. This signature is still observable in **Plate 4b**, but with a weaker magnitude. Another “warm spot” is observed at 65-67 km in November, reaching 11 K for OHP/CEL, and 8 K for TMF. This feature could already be observed in **Plates 1a to c** as a “bump” of warm temperatures in November between 60 and 70 km.

In contrast to the mid-latitudes sites, MLO (**Plate 4c**) primarily exhibits a semi-annual cycle between 25 and 80 km altitude. This is not surprising since MLO is located at 19.5°N and is influenced by the equatorial dynamical pattern which in turn is affected by both northern and southern hemispheres. The semi-annual cycle observed here is almost a continuous downward propagating oscillation with an approximate vertical speed of 12 km/month and can be identified as the thermal semi-annual oscillation (SAO). The so-called mesopause and stratopause SAOS appear here

as a combined single SAO propagating downward from the **mesopause** to 30 km with minimum amplitude at 45 km. A phase inversion is observed near 82 km similar to that observed by SME at 83 km [Garcia and Clancy, 1990]. The oscillation is strongly modulated, the first cycle being stronger than the second, The seasonal **asymmetry** of the wind and **temperature** SAO has been widely reported (**see** for example a recent wind and temperature SAO climatology by [Garcia *et al.*, 1997]). **One** explanation of this by Delisi and Dunkerton [1988] is that it is a consequence of a stronger dynamical forcing in the northern hemisphere. However, **due** to the relatively northward location of MLO, **the** late winter maxima and early summer minima of the mid-latitude annual cycle and the equatorial SAO are in phase and may also cause the first oscillation of the semi-annual cycle to **be** of larger magnitude than the second. Finally in **Plate 4c**, an annual cycle is observed below 25 km and a “cold spot” can be noted in November at 64 km at almost the same **altitude** as the previously observed “warm spot” at OHP+CEL and TMF.

### c. Annual and semiannual cycles

The annual and **semiannual** components can **be** separated by fitting the results to a multi-parameter sinusoidal function of the form:

$$T'(t, z) = T_0(z) + T_1(z) \cos \left[ \frac{2\pi(t - \varphi_1(z))}{365 \text{ days}} \right] + T_2(z) \cos \left[ \frac{2\pi(t - \varphi_2(z))}{182.5 \text{ days}} \right]$$

where  $T_1$  and  $\varphi_1$  (respectively  $T_2$  and  $\varphi_2$ ) are the amplitude (K) and phase (days) of the annual (respectively semiannual) cycle, and  $T_0$  is the annual mean temperature (K) at altitude  $z$ . The amplitudes and phases of the annual and semi-annual cycles are plotted for all sites in **Figures 1a-b and 2a-b**. The agreement **between** OHP, CEL, TMF and CSU is remarkable for both the amplitude and phase of the annual and semiannual cycles. They confirm the previous calculations performed by *Hauchecorne et al.* [1991] and also the 4 K smaller annual amplitude around 82-86 km at CSU than at OHP and CEL reported by *She et al.* [1995]. The annual cycle at these sites exhibits several maxima, of 7 K, 20 K, and 13 K located respectively at 35, 80 and 105 km, and minima located at 62 km for TMF, 65 km for OHP, and CEL, and 99 km for CSU. The minima correspond, as shown in **Figure 1b**, to the phase inversion between the stratosphere and the **mesosphere** (62-65 km), and to the altitude of the transition **between** the dynamically and radiatively-chemically driven **mesosphere** (95-100 km) also leading to a phase inversion at **thermospheric** altitudes (> 100 km). The main **difference** between TMF and the mid-latitudes sites is found in the amplitude **between** 50 and 60 km, where the TMF amplitude is smaller than for OHP and CEL. Another significant difference is the altitude of the phase inversion, about 4 kilometers lower than OHP and CEL. This can be explained using the results from **Plates 4a-c**. In these plates, the most significant fraction of the mid-latitude annual cycle occurs during **the** first six months. During these first six months, the amplitude of the TMF warm cycle has its minimum in early April at 61 km, while for OHP and CEL it has its minimum at 64-65 km. In term of phase, **between** 55 and 70 km, the TMF warm cycle propagates downward one month earlier than that at OHP and CEL, which correspond to a 4 km difference shown in **Figures 1a-b**. The shift in phase observed at TMF is due to the **influence** of the early first cycle of the low-latitudes semi-annual oscillation observed at MLO in **Plate 4c** and **Figures 2a-b**. For all mid-latitude sites, the semiannual component is weaker than the annual component, except at

the altitudes of annual phase inversion, where it reaches a maximum of 5-7 K at 60-64 km for TMF, OHP, and CEL, and more than 15 K at 105 km for CSU. The maximum at 60-64 km is due to **the** “warm spot” occurring in November at almost **the** same altitude as that of the node in the annual amplitude (3 K) occurring in early April. This is confirmed in **Figure 2b**, with **good** agreement between the early November phases at 60-64 km calculated for OHP, CEL, and TMF. The maximum at 104±2 km points **out** the interplay between the dynamically and chemically driven **mesosphere**. In June, the dynamically driven **mesosphere** has its minimum temperatures while the chemically driven **mesosphere** has its maximum, leading to moderately cold temperatures. In winter, the dynamically driven **mesosphere** seems to **extend** far higher, also leading to moderately cold **temperatures**. In spring and fall this dynamical heating is not as **efficient** as in winter, leading to colder **temperatures** than in winter and June. The resulting seasonal variation of the temperature at 104±2 km is an apparent semiannual cycle, with maxima in **winter** and summer, and minima in spring and fall.

f. 2-to 30-day temperature variability

Having established the **climatological** average, it is now interesting to look at the temperature variability on shorter time scales. Since most of the initial profiles were integrated over several hours or even over a night, a large part of the variability due to gravity waves has already been removed by this averaging. Thus, if the standard deviation of each daily composite profile from a 33-day averaged profile is calculated, an indicator of the wave activity of all atmospheric waves with periods **between** 2 and 33 days is obtained. These include most of **inertio-gravity** waves and planetary waves. In contrast to OHP, CEL and CSU, where most of the gravity waves with periods shorter than 24 hours are removed, periods between 4 and 24 hours may sometimes be included for TMF and MLO. Of course, the statistical error associated with the **lidar** measurements should be small enough compared to the variance associated with the waves if **we** want to extract a significant geophysical signature. This is not the case in the upper part of the profiles. For this reason a simple filter, a function of altitude and constant in time, was applied to the **data**. The growth rate of the filter coefficients is related to the atmospheric scale height since the statistical error is a function of the photon counts, i.e. the atmospheric density. The filter was computed with the assumption of a 10 K statistical error at the altitude of 93 km and a 7 km mean atmospheric scale height. Though not optimized, this filter will remove most of the variance due to instrumental noise in the upper part of the profiles without removing the geophysical information. The filtered standard deviations from the 33-day average are **plotted** in **Plates 5a to 5c** for OHP+CEL, CSU, TMF, and MLO. For CSU, the data are filtered with a 10 K statistical error assumption taken at 112 km instead of 93 km. By comparing all 3 plates, it is clear that the variability with periods between 2 and 33 days has its maximum at mid-latitudes and **decreases** significantly towards the tropical latitudes. Despite the different methods of vertical filtering and the different integration periods of each instrument, the qualitative and quantitative agreement and consistency are remarkable. As **expected**, and as previously shown by *Hauchecorne et al. [1991]*, the maximum wave activity at mid-latitudes appears in winter. In the stratosphere, a winter maximum of 10-12 K occurs between 35 and 45 km at OHP/CEL (**Plate 5a**), (50% smaller at TMF, **Plate 5b**). **This** maximum is principally associated with stratospheric warmings, and certainly associated with all further **inertio-gravity** and planetary wave activity. **After** the observed maximum of 10 K around 40 km, and a minimum of 8 K at 55 km, a second winter maximum of 12 K is observed in the **mesosphere** at OHP+CEL (50% smaller at TMF) between 70 km

and 95 km. Then a second minimum occurs around 100 km. The **mesospheric** maximum is associated with the **mesospheric** temperature inversions whose amplitude can frequently reach 40 K, with a 1- to 5-day averaged duration (scc for example [*Leblanc and Hauchecorne, 1997a*]). However, due to the basic **filter** applied here to remove the instrumental noise it is not clear where the **mesospheric** maximum actually occurs and what is its actual magnitude. The most important result is that OHP and CSU are in very good **agreement** again, even quantitatively (Plate 5a), and that a maximum of 2- to 33-day variability is observed around 75 km, associated with the **mesospheric** temperature inversions.

In summer, the standard deviation is very low, even at mid-latitudes, confirming the weak wave activity during this season at these latitudes. Two **secondary** maxima are **nevertheless** observed in early May and early September around 80 km at OHP, while late March and **late September** appear to be the quietest periods of the year. At MLO (**Plate 5c**), the **extratropical** planetary waves are too far away to account for the temperature variability, except in the upper stratosphere in **December**. Greater activity is also observed in the lower stratosphere, showing the high variability of the tropical **tropopause**. In the mesosphere, two maxima are observed, following a remarkable symmetrical pattern with six months interval. First reaching 8 K before the equinoxes, they reach 10 K in early May and November at 83 km.

#### g. Seasonal evolution of the temperature

In order to characterize the seasonal temperature variations the temporal evolution of the temperature, i.e. the time derivative, was calculated:

$$T'(t,z) = \frac{\delta T}{\delta t} = \frac{T'(t+1, z) - T'(t-1, z)}{d(t+1, z) - d(t-1, z)}$$

where  $d(t)$  and  $d(t+1)$  are two **consecutive** days of measurement (not necessarily two consecutive dates). The results are presented in **Plates 6a to 6c** for the lidar profiles at OHP+CEL, CSU, TMF, and MLO, and in **Plates 6d to 6f** for the CIRA-86 equivalent. As for the previous plates, CSU and OHP+CEL are plotted together, with the OHP+CEL data below 85 km and the CSU data above. The lidar profiles are plotted with a 10-day time resolution and are smoothed over 3 points so that the information appears here as quasi-monthly mean values allowing a better comparison with CIRA. Once again, the **agreement** between OHP+CEL and CSU is remarkable.

At **mesospheric** and stratospheric mid- and subtropical latitudes (**Plates 6a and 6b**), the **summertime** temperature variations are quite small below 75 km with a maximum cooling rate of 4 K/month below 75 km, while the wintertime evolution is much more chaotic. Above 75 km the entire year looks chaotic with cooling rates greater than  $\pm 8$  K/month. Non-negligible instrumental noise may **contribute** to the larger variability at these altitudes. However, it is clear that the summer upper **mesosphere** cools down in two steps. The first step is in February around 85 km, with a maximum cooling rate of 12 K/month, and the second step in late April around 75 km and above. All mid-latitudes instruments (i.e. OHP, CEL, CSU and TMF) agree in this **part**. Then, a **first** strong heating period takes place in late August ( $>14$  K/month as shown in **Plate 6a**). This **mesospheric** warming propagates downward, with a maximum of 10 K/month at 65 km in mid-October. **Immediately after** this warming period, a short quiet period

follows, extending from September around 85 km to late October at 70 km. Then a second strong warming period occurs, with a maximum of 10 K/month at 90 km in October propagating downward with a maximum of 6 K/month in early November. Then, from late November to late December, the temperature behavior in the **mesosphere** is driven by the occurrence of the **mesospheric** temperature inversions. A large cooling (up to -14 K/month) is observed around 65 km and a moderate warming (+7 K/month) is observed at 75 km. This is in good agreement with some modeling performed by [*Leblanc and Hauchecorne, 1997 b*]. In the stratosphere the winter cooling occurs in a **regular** manner in October (-4 to -8 K/month) in the entire 30-55 km layer.

For MLO (**Plate 6c**), the semiannual oscillation is characterized by weak warming rates (maximum 4 K/month at 38 and 45 km in January and August respectively) and cooling rates (around 2 K/month) in the entire middle atmosphere except the upper **mesosphere**. Above 75 km, stronger values (up to 15 K/month) randomly distributed in time are observed. Once again, a possible explanation is the effect of the **mesospheric** tides. At these altitudes, the amplitude of the diurnal and semidiurnal tides can reach 5-10 K. However, the different times of measurements do not vary critically (typically, all measurements are obtained within the first 5 hours of the night). Some other effects related to an insufficient statistics and/or residual noise have to be taken into account. A longer database may lead to significant insights in the future.

For TMF (**Plate 6b**), an **expected intermediary scheme between OHP+CEL and MLO** is observed. The mid-latitude annual cycle is dominant but with some modulation due to the influence of the lower latitudes. For example, the early winter cooling of the stratosphere occurs at the same time as for OHP+CEL (late October), and the summer cooling in the **mesosphere** behaves like at OHP+CEL. The first strong winter **mesospheric** warming observed on **Plate 6a** is also observed for TMF but with weaker amplitude (+8 K/month at 67 km). Then the winter **mesosphere** behaves quite differently. The strong cooling period between 55 and 65 km occurring from November to December at OHP+CEL, now occurs in late December to early January nearer to 55 km altitude. In addition, the strong warming period observed at OHP at 75 km is no longer observed in December but in February and at 70 km. The lower latitudes seem to affect significantly the temperature behavior at TMF during this period. The 4 K/month cooling rate in mid-October at 60 km observed at MLO is in opposite phase with the 10 K/month warming rate observed at 65 km at OHP. The consequence is a moderate warming rate of 4 K/month at TMF. Also, a 6 K/month warming rate observed at MLO at 65 km in early December is in opposite phase with the large 14 K/month cooling rate observed at OHP, resulting in a moderate 6 K/month cooling rate at TMF.

## 5. Discussion and conclusion.

When studied all together, **Plates 1, 2, 3, 4, 5**, and especially **plates 6**, allow important new insights in the middle atmospheric temperature climatology. Most of the differences with the CI RA-86 climatology can be explained as can most of the **differences** observed between some instruments.

As has been observed in all previous middle atmospheric temperature climatologies [*Garcia and Clancy, 1990, Hauchecorne et al., 1991; Bills and Gardner, 1993; Clancy et al., 1994; Yu and She, 1995, Garcia et al., 1997*], a dominant annual cycle is observed at mid-latitudes and a semiannual cycle is dominant at lower latitudes. Below 60

km the annual cycle is in phase with the solar flux leading to a warm summer and cold winter stratosphere and lower mesosphere, as expected. Between 65 and 95 km, the annual cycle is in opposite phase to the solar flux, as a consequence of a dynamically driven mesosphere, and is characterized by a warm winter and cold summer mesosphere. Above 102 km, thermospheric processes lead again to an annual cycle that is in phase with the solar flux. The observed downward propagating temperature behavior in the mesosphere points out the dominant wave driven pattern, in contrast with the vertically stationary behavior observed below 50-55 km. At MLO the dominant semi-annual cycle is modulated by the northern mid-latitude annual cycle thus contributing, together with the well known seasonally asymmetric equatorial SAO, to the first warm-cold cycle (winter and spring) being stronger than the second (summer and fall).

The 2-33 day variability shown in this climatology is also in good agreement with that shown in a previous climatology [Hauchecorne et al., 1991]. A maximum in the planetary wave activity is observed in winter in the stratosphere and the maximum variability is also observed in the winter mesosphere due to the occurrence of the temperature inversions. An important latitudinal gradient is also observed with decreasing variability from the mid- to the lower-latitudes.

Systematic departures from the CIRA-86 model were observed which confirms the similar results of previous comparisons [Hauchecorne et al., 1991; Clancy et al., 1994]. In particular, too cold temperatures in the CIRA-86 model lead to a large difference ( $> 15$  K) around 90-95 km compared to lidar results, possibly due to an overestimation of non-LTE effects in the computation of the CIRA-86 temperatures [Lawrence and Randel, 1996]. On an annual basis, CIRA-86 seems to be too warm around 55-60 km, too cold between 60 and 75 km, too warm between 75 and 85 km, and much too cold around 90-95 km. Above 100 km the high temperature variability caused by thermospheric processes leads to a large negative departure of 16 K in summer. Consequently, between 95 and 105 km, the vertical gradient of the temperature difference CSU-CIRA is extremely steep in summer, reaching  $-3.4$  K/km (see top of Plate 3a), illustrating the poor accuracy of the CIRA-86 model in this region. Using too cold CIRA-86 temperatures at 90-95 km for initialization can lead to some dramatic temperature errors at the very top of the Rayleigh lidar profiles. For this reason, the CNRS/SA and JPL lidar groups are currently investigating the use of a different a priori temperature information to avoid such uncertainty.

When the seasonal variation of temperature at mid-latitudes is studied more in detail some new interesting results are obtained. Instead of a steadily cooling spring and a steadily warming fall in the mesosphere (as predicted by the vertically and temporally smoothed CIRA-86 model) some short periods of strong cooling and warming are observed. It appears that the cooling of the summer mesosphere is characterized by two short periods of strong cooling occurring in late January at 85 km and in April-May between 80 and 85 km. The warming of the winter mesosphere occurs suddenly in late August at 85 km and then propagates slowly downward, reaching altitudes of 65-70 km in October. A second warming period occurs at 85 km in October. In the lower and middle mesosphere (55-80 km) a dramatic event disturbs the well-defined mid-latitude winter mesosphere warming. In late November and December a strong cooling period occurs around 60-65 km together with a weak warming period at 75 km, more than two months after the initial winter warming at that height. This is the strong signature of the so-called

mid-latitude **mesospheric** temperature inversions. The observed **phenomenology** of these inversions is in **agreement** with some **numerical** modeling performed by **Leblanc and Hauchecorne [1997b]** in which adiabatic cooling around 65 km together with adiabatic heating around 75 km were able to produce temperature inversions at mid-latitudes. Above TMF the **mesospheric** temperature inversions appear to occur 1 to 2 months later than above OHP and CEL, as a consequence of **the** latitudinal variability. These winter mid-latitude **temperature** inversions around 70 km should not **be** confused with the **equinoctial** low-latitude inversions observed around 80 km by **SME [Clancy et al., 1994]**, **ISAMS**, and **HALOE [Leblanc and Hauchecorne, 1997a]**, and by **lidar** at MLO, where **the** SAO [Clancy et al., 1994; Garcia and Clancy, 1990], the tides, and/or chemical heating [Meriwether and Mlynczak, 1995] may play a more important role.

The chaotic nature of the seasonal variations of the middle atmospheric temperature allows most of the discrepancies observed between the different measurement sites, or between the **lidar** and **CIRA-86** climatologies, to be explained. Above TMF, the large positive departure from **CIRA-86** in February is due to the second winter warming where the occurrence of the **mesospheric temperature** inversions has **its** maximum. The positive departure at 60 km in April and 60-70 km in **late fall** are related respectively to the late winter warming (February-March) and to the first winter warming (October). The negative maximum at 75-80 km is related to the stationary period trapped in October between the first and second winter warmings. Above MLO, **it** is not unlikely that most of the observed departure in the middle and upper **mesosphere** is related to tidal effects and/or **the mesopause thermal SAO**. The amplitudes of 1-5 K **predicted** by tidal models [Hagan, 1996] may **be underestimated** [Keckhut et al., 1996] and this will be investigated in more detail during the next months.

The climatology presented in this paper was obtained using composite temperature profiles from several years of measurements. Of course, a non-negligible **interannual** variability may disturb the temperature **field** from year to year. However, the trends already observed in previous **climatologies [Hauchecorne et al., 1991][Hood et al., 1993]** remain small compared to the seasonal variations. Also, the **effect** of volcanic eruptions, such **Pinatubo** in 1991 [Keckhut et al., 1995] and more recently **Soufrière** on **Montserrat**, may have non-negligible disturbing effects. All trends, 11-year solar cycle, Quasi Biennial Oscillation (**QBO**), and volcanic eruption effects are currently being investigated and an overall climatology of the middle atmospheric temperature may be obtained within few months. The use of such a complete climatology is crucial for many purposes such as providing a reference atmosphere for models and instruments, a background atmosphere for smaller scale studies, an overall comprehension of **the** strongly coupled lower-middle-upper atmosphere, and more. To this date, only a **few** instruments can provide such long-term data series. With the **recent** and future development of many ground based **lidars** within the NDSC at many **latitudes**, a more complete climatology of the middle atmospheric **temperature** should be available within few years.

#### **Acknowledgements:**

**The** work described in **this** paper was carried out, in **part**, at the Jet Propulsion Laboratory, California Institute of Technology, under an agreement with the National Aeronautics and Space Administration. TL thanks the National Research Council for the award of an **associateship**.

## References:

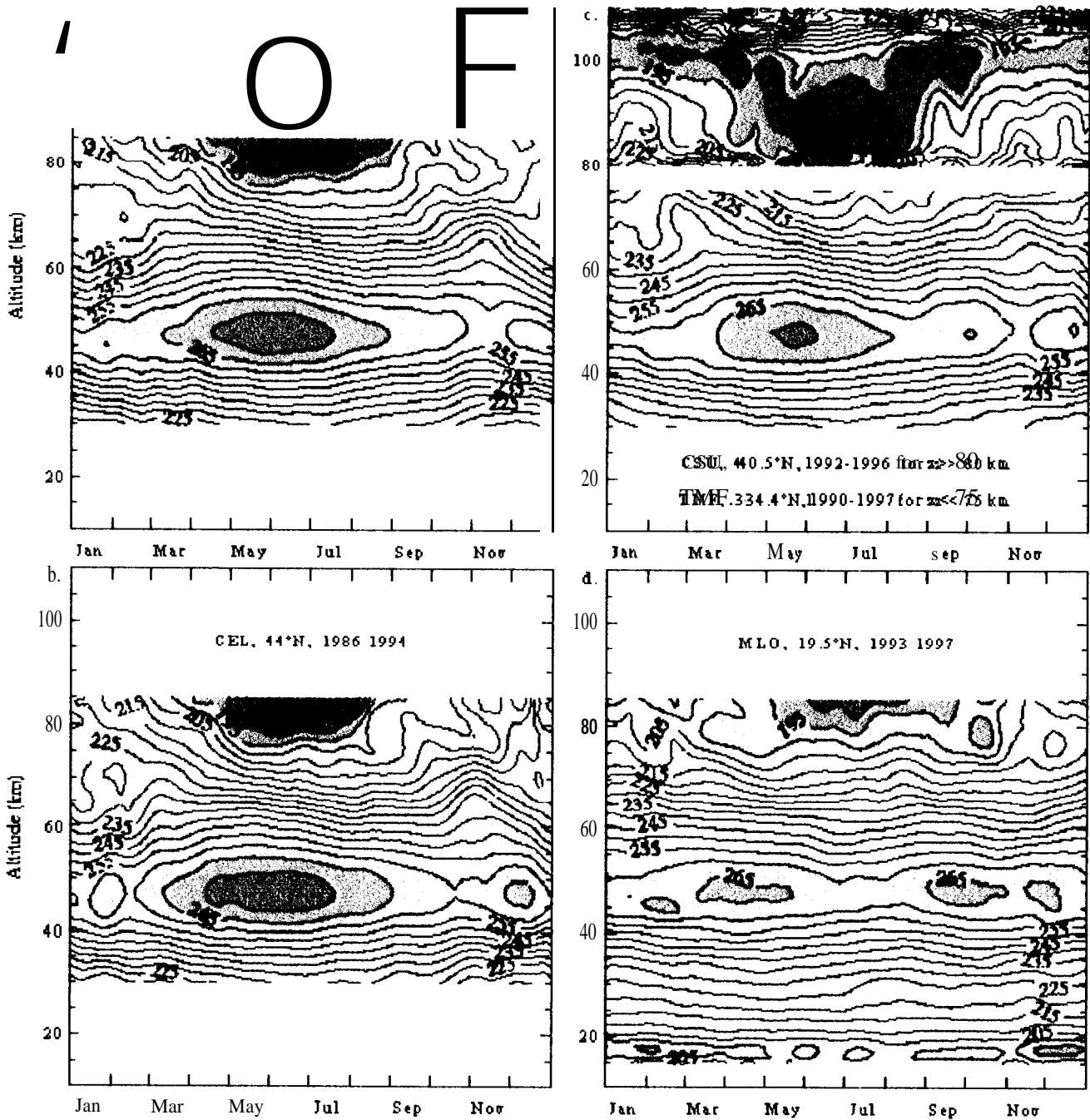
- Barnett, J. J. and M. Corney, Middle atmosphere reference model derived from satellite data, in *Handbook for MAP*, vol. 16, edited by K. Labitzke, J. J. Barnett, and B. Edwards, pp. 47-137, University of Illinois, Urbana, 1985.
- Bills, R. E., and C. S. Gardner, Lidar observations of the mesopause region temperature structure at Urbana, *J. Geophys. Res.*, 98, 1011-1021, 1993.
- Chanin, M. L., A. Hauchecorne, N. Spires, Contribution to the new reference atmosphere from ground-based lidar, *Adv. Space Res.*, 10, 211-216, 1990.
- Clancy, R. T., and D. W. Rush, Climatology and trends of mesospheric (58-90 km) temperature based upon 1982-1986 SME limb scattering profiles, *J. Geophys. Res.*, 94, 3377-3393, 1989.
- Clancy, R. T., D. W. Rush, and M. T. Callan, Temperature minima in the average thermal structure of the middle atmosphere (70-80 km) from analysis of 40- to 92-km SME global temperature profiles, *J. Geophys. Res.*, 99, 19,001-19,020, 1994.
- Curtis, P. D., J. T. Houghton, G. D. Peskett, and C. D. Rodgers, The Pressure Modulator Radiometer for Nimbus F, *Proc. R. Soc. London, Ser. A*, 337, 135-150, 1974.
- Delisi, D. P., and T. J. Dunkerton, Seasonal variation of the semiannual oscillation, *J. Atmos. Sci.*, 45, 2772-2787, 1988.
- Derr, V.E., and C.G. Little, A comparison of remote sensing of the clear atmosphere by optical, radio, and acoustic radar techniques, *Appl. Opt.*, 9, 1976-1992, 1970.
- Donovan, D. P., J. A. Whiteway, and A. I. Carswell, Correction for non-linear photon-counting effects in lidar systems, *Appl. Opt.*, 32, 6742-6753, 1993.
- Ellis, P., et al., The selective chopper radiometer for Nimbus 5, *Proc. R. Soc. London, A*, 334, 149-170, 1973.
- Elterman, L. B., The measurement of stratospheric density distribution with the searchlight technique, *J. Geophys. Res.*, 56, 509-520, 1951.
- Fishbein, E. F., R. E. Cofield, L. Froidcvaux, R. F. Jarnot, T. Lungu, W. G. Read, Z. Shippony, J. W. Waters, I. S. McDermid, T. J. McGCC, U. Singh, M. Gross, A. Hauchecorne, and M. E. Gelman, Validation of UARS Microwave Limb Sounder temperature and pressure measurements, *J. Geophys. Res.*, 101, 9983-10,016, 1996.
- Fleming, E. L., S. Chandra, J. J. Barnett and M. Corney, COSPAR International Reference Atmosphere, Chapter 2: Zonal mean temperature, pressure, zonal wind and geopotential height as functions of latitude, *Adv. Space Res.*, 10 (12), 11-59, 1990.
- Garcia, R. R., and R. T. Clancy, Seasonal Variation in equatorial mesospheric temperatures observed by SME, *J. Atmos. Sci.*, 47, 1666-1673, 1990.

- Garcia, R. R., T. J. Dunkerton, R. S. Lieberman, and R. A. Vincent, Climatology of the semiannual oscillation of the tropical middle atmosphere, *J. Geophys. Res.*, *accepted*, 1997.
- Gille, J. C., J. M. Russell III, P. L. Bailey, L. L. Gordley, E. E. Remsberg, J. H. Lienesch, V. W. G. Planck, F. B. House, L. V. Lyjak, and S. A. Beck, Validation of temperature retrievals obtained by the Limb Infrared Monitor of the Stratosphere (LIMS) experiment on Nimbus 7, *J. Geophys. Res.*, *89*, 5147-5160, 1984.
- Gille, J. C., P. L. Bailey, S. T. Massie, L. V. Lyjak, D. P. Edwards, A. E. Roche, J. B. Kumer, J. L. Mergenthaler, M. R. Gross, A. Hauchecorne, P. Keckhut, T. J. McGee, I. S. McDermid, A. J. Miller, and U. Singh, Accuracy and precision of cryogenic limb array etalon spectrometer (CLAES) temperature retrievals, *J. Geophys. Res.*, *101*, 9583-9602, 1996.
- Hagan, M. E., Comparative effects of migrating solar sources on tidal signatures in the middle and upper-atmosphere, *J. Geophys. Res.*, *101*, 21,213-21,222, 1996.
- Hedin, A. E., A revised thermospheric model based on mass spectrometer and incoherent scatter data: MSIS-83, *J. Geophys. Res.*, *88*, 10,170-10,188, 1983.
- Hauchecorne, A., and M. L. Chanin, Density and Temperature Profiles obtained by lidar between 35 and 70 km, *Geophys. Res. Lett.*, *7*, 565-568, 1980
- Hauchecorne, A., M. L. Chanin, and P. Keckhut, Climatology and trends of the middle atmospheric temperature (33-87 km) as seen by Rayleigh lidar over the south of France, *J. Geophys. Res.*, *96*, 15,297-15,309, 1991.
- Hauchecorne, A., M. L. Chanin, P. Keckhut and D. Nedeljkovic, LIDAR monitoring of the temperature in the middle and lower atmosphere, *Appl. Phys.*, *B55*, 29-34, 1992
- Hood, L. L., J. L. Jirikovic, and J. P. McCormack, Quasi-decadal variability of the stratosphere: Influence of long-term solar ultraviolet variations, *J. Atmos. Sci.*, *50*, 3941-3958, 1993.
- Keckhut, P., M. L. Chanin, and A. Hauchecorne, Stratosphere temperature measurement using Raman lidar, *Appl. Opt.*, *29*, 5182-5186, 1990.
- Keckhut, P., A. Hauchecorne, and M. L. Chanin, A critical review of the database acquired for the long-term surveillance of the middle atmosphere by French Rayleigh lidars, *J. Atmos. Oceanic Technol.*, *10*, 850-867, 1993.
- Keckhut, P., A. Hauchecorne, and M. L. Chanin, Midlatitude long-term variability of the middle atmosphere: Trends and cyclic and episodic changes, *J. Geophys. Res.*, *100*, 18,887-18,897, 1995.
- Keckhut, P., Gelmann M. E., Wild J. D., Tissot F., Miller A. J., Hauchecorne A., Chanin M.-L., Fishbein E. F., Gille J., Russell III J. M., and Taylor F. W., Semi-diurnal and diurnal tides (30-55 km): Climatology and effect on UARS-LIDAR data comparisons, *J. Geophys. Res.*, *101*, 10299-10310, 1996.
- Kent, G. S., and R. W. Wright, A review of laser radar measurements of atmospheric properties, *J. Atmos. Terr. Phys.*, *32*, 917-943, 1970.

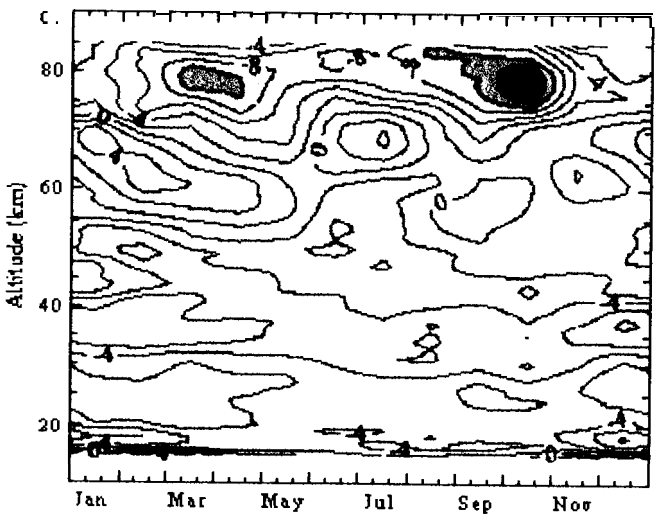
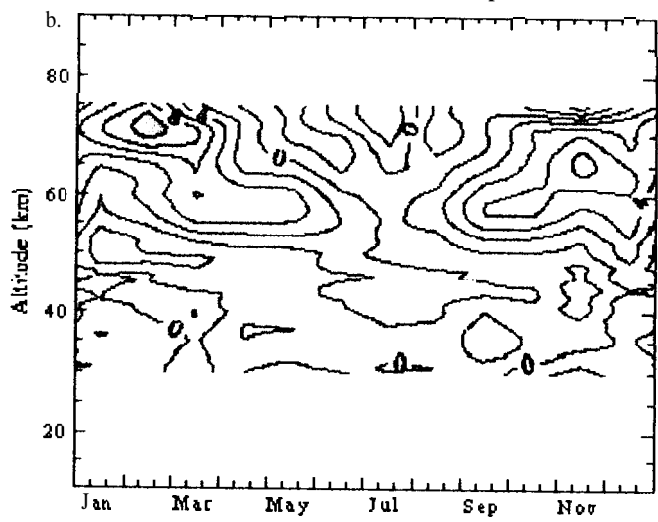
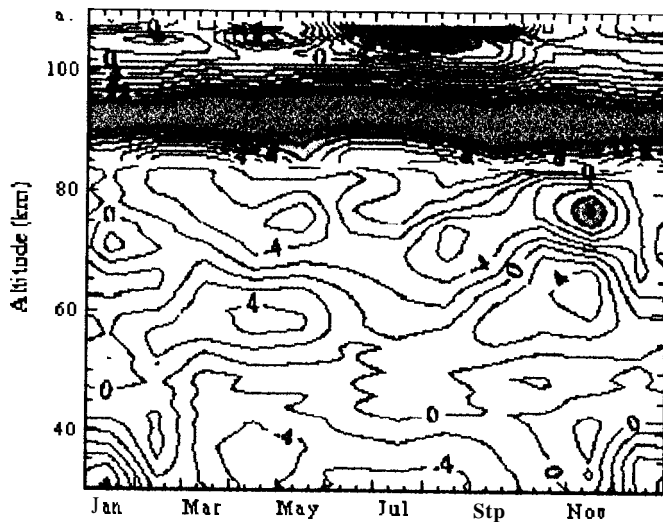
- Labitzke, K., and J. J. Barnett, Review of the radiance distribution in the upper **mesosphere** as observed from the Nimbus 6 pressure modulator radiometer (PMR), *Planet. Space Sci.*, 29,673-685, 1981.
- Leblanc, T., and A. Hauchecorne, Recent observations of the **mesospheric** temperature inversions, *J. Geophys. Res.*, 102, 19,471-19,482, 1997a,
- Leblanc, T., I. S. McDermid, A. Hauchecorne, and P. Keckhut, Evaluation and optimization of **lidar** temperature analysis algorithms using simulated data, submitted JGR, 1997.
- Leblanc, T., and A. Hauchecorne, 2-D numerical modeling of the **mesospheric** temperature inversions, Submitted, JASTP, 1997b.
- Lawrence, B. N., and W. J. Randel, Variability in the **mesosphere** observed by the Nimbus 6 pressure modulator radiometer, *J. Geophys. Res.*, 101, 23,475-23,489, 1996.
- McDermid, I. S., T. D. Walsh, A. Deslis and M. L. White, Optical systems design for a stratospheric **lidar** system, *Appl. Opt.*, 34,6201-6210, 1995.
- Meriwether, J. W., and M. G. Mlynczak, Is chemical heating a major cause of the **mesosphere** inversion layer ?, *J. Geophys. Res.*, 100, 1379-1387, 1995.
- Rodgers, C. D., R. L. Jones, and J. J. Barnett, Retrieval of temperature and composition from NIMBUS 7 SAMS measurements, *J. Geophys. Res.*, 89, 5280-5286, 1984.
- Miller, D. E., J. L. Brownscombe, G. P. Carruthers, D. R. Pick, and K. H. Stewart, operational temperature sounding of the stratosphere, *Philos. Trans. R. Soc. London, Ser. A*, 296, 65-71, 1980.
- Russell, J. M., III, L. L. Gordley, J. H. Park, S. R. Drayson, W. D. Hesketh, R. J. Ciccone, A. F. Tuck, J. E. Frederick, J. E. Harries, and P. J. Crutzen, The Halogen Occultation Experiment, *J. Geophys. Res.*, 98, 10,777-10,797, 1993.
- Scnft, D. C., G. C. Papen, C. S. Gardner, J. R. Yu, D. A. Krueger, and C. Y. She, Seasonal variations of the thermal structure of the **mesopause** region at Urbana, IL (40°N, 88°W) and Ft. Collins CO (41°N, 105°W), *Geophys. Res. Lett.*, 21, 821-824, 1994
- Schmidlin, F. J., Repeatability and measurement uncertainty of United States meteorological **rocketsondes**, *J. Geophys. Res.*, 86,9599-9603, 1981.
- She, C. Y., J. R. Yu, and D. A. Krueger, Vertical structure of the **midlatitude** temperature from stratosphere to **mesopause** (30 -105 km), *Geophys. Res. Lett.*, 22, 377-380, 1995.
- Taylor, F. W., et al., Remote sensing of atmospheric structure and composition by pressure modulator radiometry from space: The ISAMS experiment on UARS, *J. Geophys. Res.*, 98, 10,799-10,814, 1993.
- Yu, J. R., and C. Y. She, Climatology of a **midlatitude mesopause** region observed by a **lidar** at Fort Collins, Colorado (40.6°N, 105°W), *J. Geophys. Res.*, 100,7441-7452, 1995.

Data set	OHP	CEL	Csu	TMF	MLo	
Longitude	6.0° E	<b>1.0° W</b>	105.0° w	117.7° w	155.6° W	
Latitude	44.0° N	44.0° N	40.6° N	34.4° N	19.5° N	
Emitted/Rcccived wavelength (rim)	532/532	532/532	589/589	353/353	353/353-385	
Laser energy (mJ/pulse)	400	200	30	50	50	
Laser frequency (pulse/s)	50	30	20	150	200	
Telescope area (m <sup>2</sup> )	0.7810.03	1.44	0.1	0.64	0.78	
Field of view ( <b>mr</b> ad)	0.2510.55	0.2	<b>1.0</b>	2.0	1.0	
Vertical resolution used	1 km	<b>1km</b>	<b>1 km</b>	1 km	1 km	
Altitude Range used (km)	30-85	30-85	85-105	32-75	15-85	
Estimated error at mid-range	< 1 K	< 1 K	-0.5 K	< 1 K	< 1 K	
Estimated statistical error at top	- 5 K	~ 5 K	- 3 K	~ 5 K	~ 5 K	
First year used	1984	1986	1992	1990	<b>1993</b>	
Last year used	1995	<b>1994</b>	1996	1997	1997	
Number of profiles:	Total	1244	670	249	686	411
January	153	60	<b>16</b>	50	39	
February	109	62	26	39	31	
March	129	78	23	50	44	
April	79	50	17	70	48	
May	65	45	11	58	38	
June	<b>81</b>	46	16	83	40	
July	108	56	28	63	17	
August	99	41	24	46	39	
<b>September</b>	90	70	19	58	28	
October	82	<b>57</b>	24	69	32	
November	119	58	23	58	30	
December	130	<b>47</b>	22	42	25	

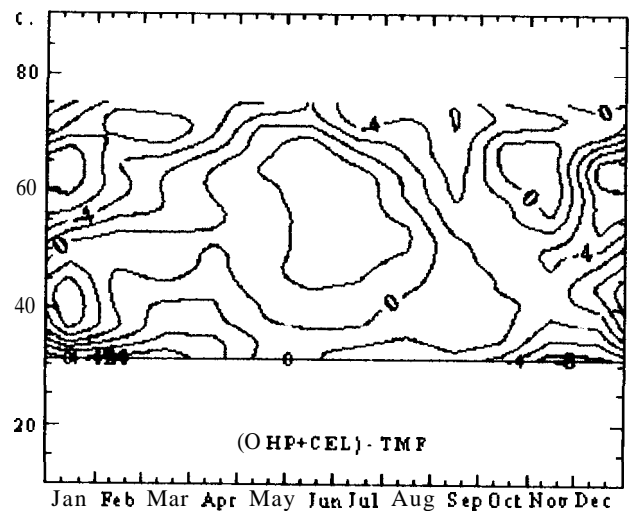
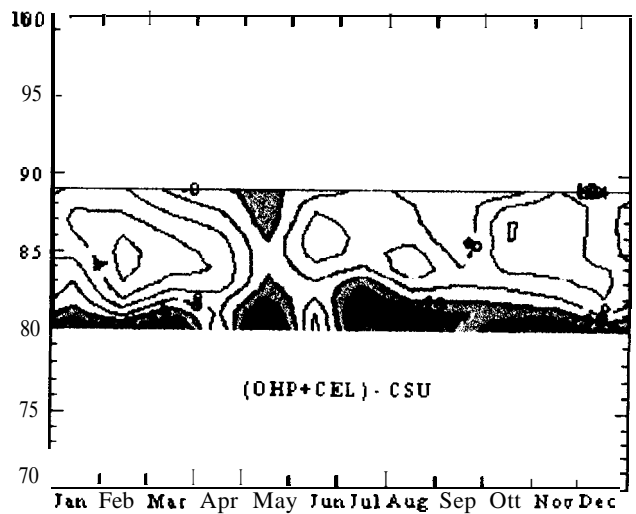
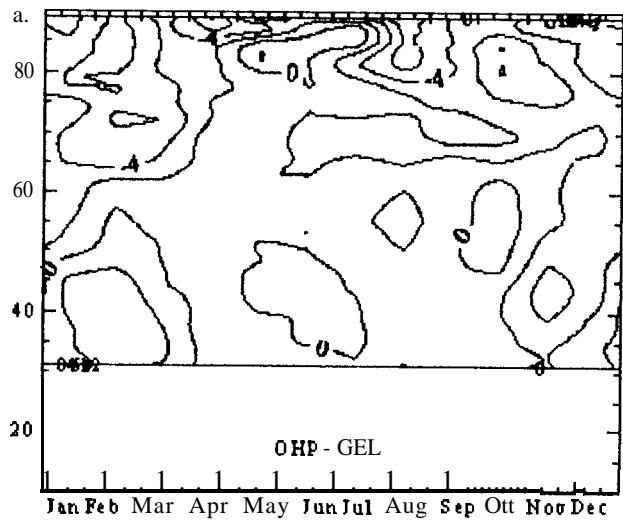
**Table 1:** Instrumental and data set characteristics used in this climatology (individual profiles).



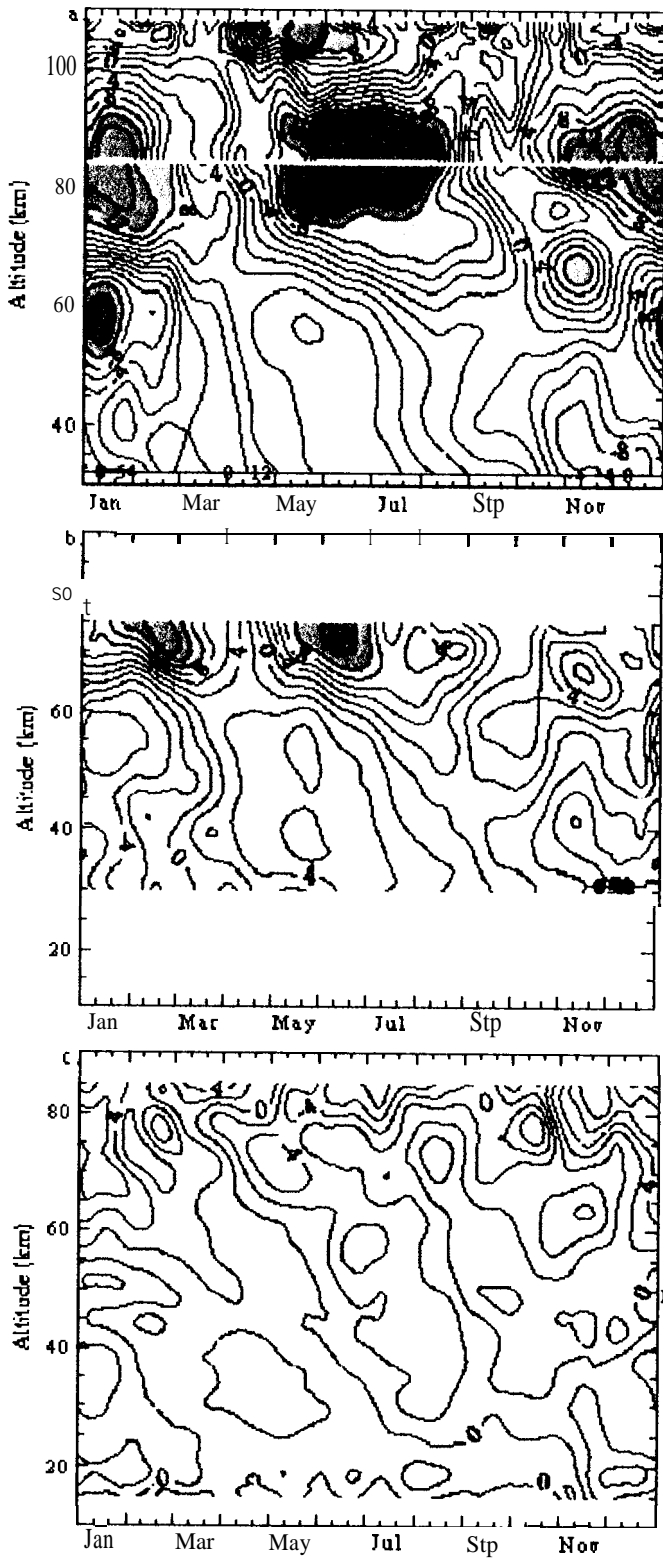
**Plates 1.** Climatological temperatures obtained from lidar measurements at: (a) OHP (44°N, 6°E), (b) CEL (44°N, 1°W), (c) CSU (40.5°N, 105°W) and TMF (34.4°N, 117.7°W), and (d) MLO (19.5°N, 155.6°W). The color scale extends from 180 K (mauve) to 280 K (dark red), contour interval: 5 K,



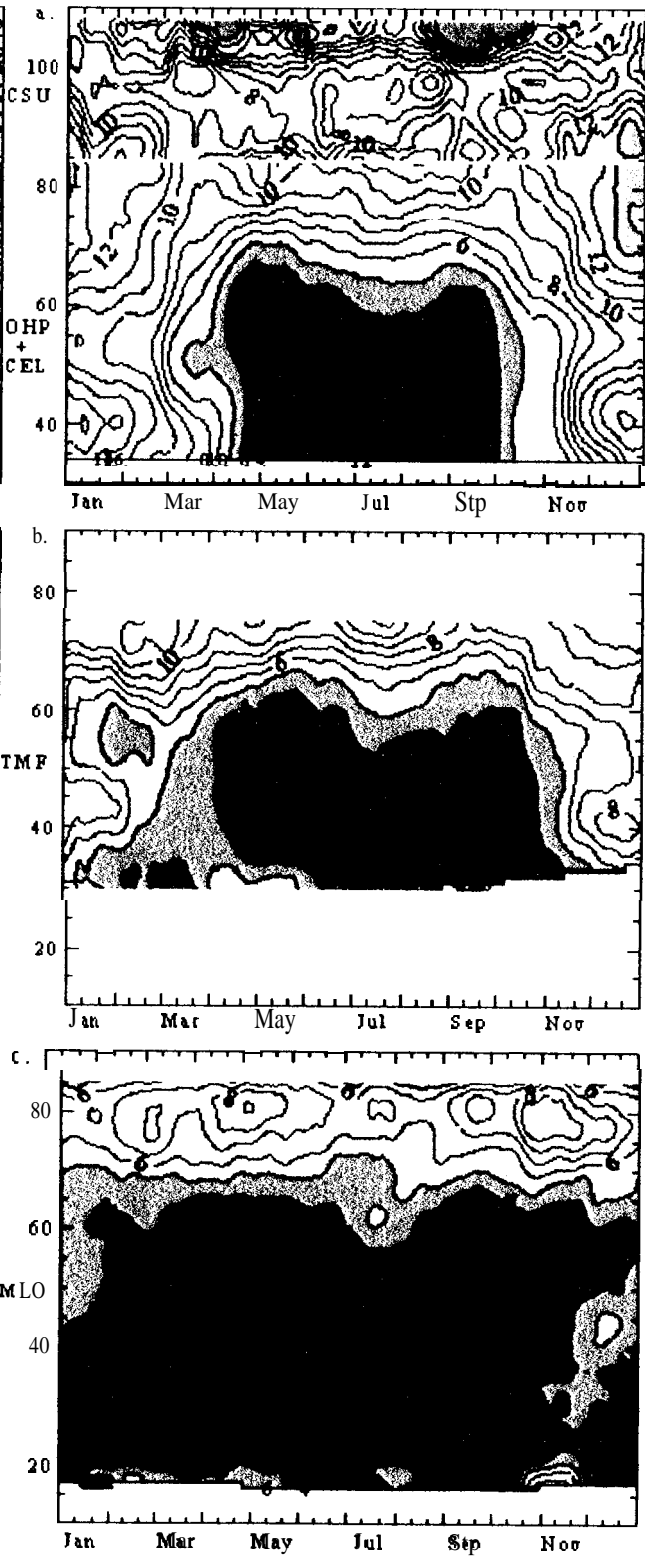
**Plates 3.** Monthly mean departure from the CIRA-86 temperatures obtained for: (a) OHP+CEL and CSU, (b) TMF, and (c) MLO. Contour interval is 2 K.



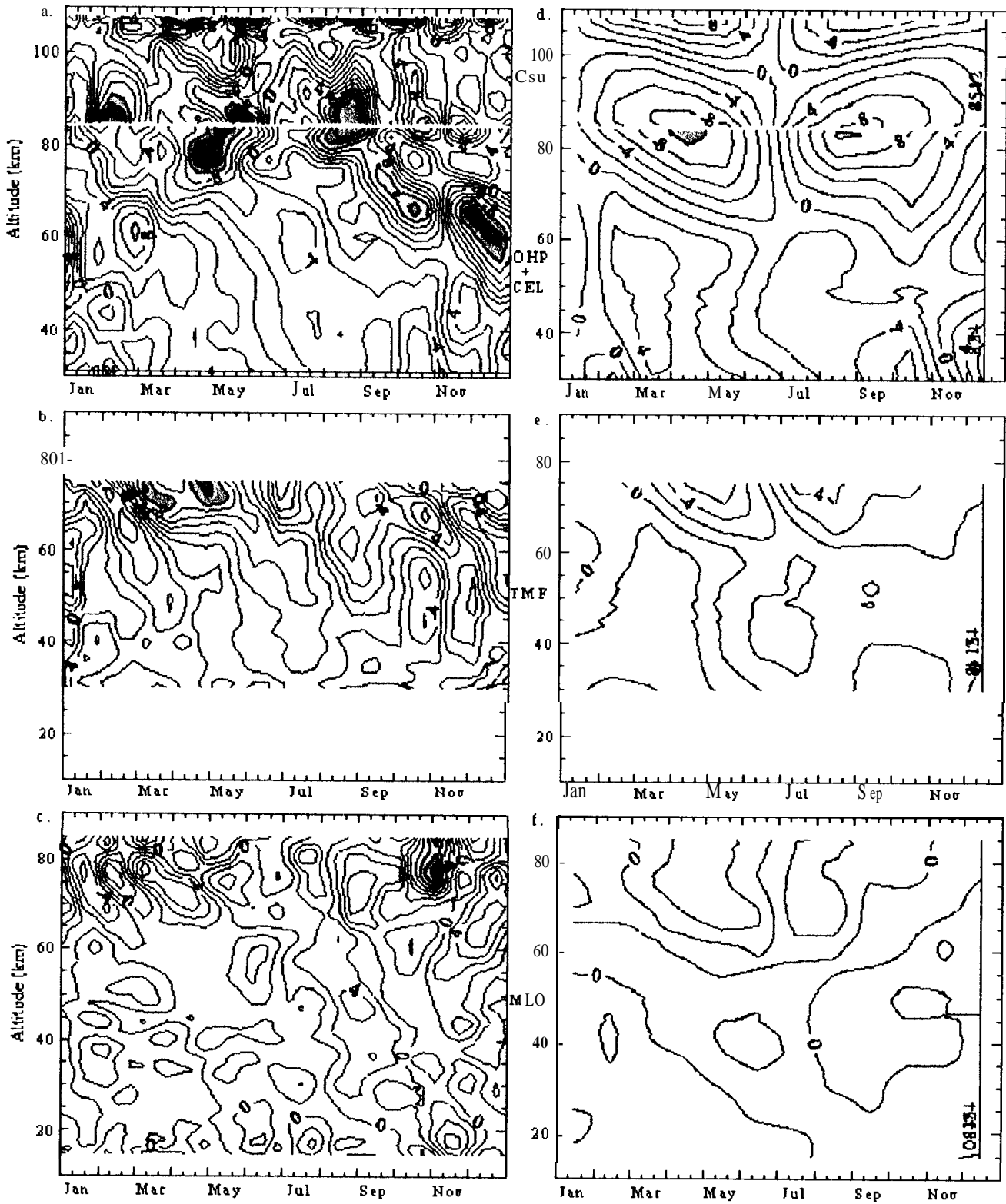
**Plates 2.** Temperature differences (K) between (a) OHP and CEL, (b) OHP+CEL and CSU, and (c) OHP+CEL and TMF obtained from the climatological values given in Plates 1, Contour interval is 2 K.



**Plates 4.** Daily mean deviation from the annual mean temperature (calculated from the climatological temperature shown in Plates 1, (a) OHP+CEL and CSU, (b) TMF, (c) MLO. Contour intervals: 2 K.



**Plates 5.** Daily mean standard deviation from 33-days mean temperature (K) at (a) OHP+CEL and CSU, (b) TMF and (c) MLO. Contour intervals: 1 K.



**Plates 6.** Time evolution of temperature (K/month) calculated from the climatological temperatures given in Plates 1 (left panels), and calculated from the CIRA-86 monthly mean temperatures (right panels). For the left panels, time resolution is 10 days, and data are smoothed over 3 points, (a) OHP+CEL and CSU, (b) TME, and (c) MLO. Contour intervals: 2 K/month.